CLIMATOLOGY

North Atlantic cooling triggered a zonal mode over the Indian Ocean during Heinrich Stadial 1

Xiaojing Du[1,2]*, James M. Russell[1,2], Zhengyu Liu[3], Bette L. Otto-Bliesner[4], Delia W. Oppo[5], Mahyar Mohtadi[6], Chenyu Zhu[7], Valier V. Galy[8], Enno Schefuß[6], Yan Yan[9], Yair Rosenthal[10], Nathalie Dubois[11,12], Jennifer Arbuszewski[5], Yu Gao[13]

Abrupt changes in the Atlantic meridional overturning circulation (AMOC) are thought to affect tropical hydroclimate through adjustment of the latitudinal position of the intertropical convergence zone (ITCZ). Heinrich Stadial 1 (HS1) involves the largest AMOC reduction in recent geological time; however, over the tropical Indian Ocean (IO), proxy records suggest zonal anomalies featuring intense, widespread drought in tropical East Africa versus generally wet but heterogeneous conditions in the Maritime Continent. Here, we synthesize proxy data and an isotope-enabled transient deglacial simulation and show that the southward ITCZ shift over the eastern IO during HS1 strengthens IO Walker circulation, triggering an east-west precipitation dipole across the basin. This dipole reverses the zonal precipitation anomalies caused by the exposed Sunda and Sahul shelves due to glacial lower sea level. Our study illustrates how zonal modes of atmosphere-ocean circulation can amplify or reverse global climate anomalies, highlighting their importance for future climate change.

INTRODUCTION

The tropical ocean-atmosphere circulation exerts a profound influence on the global climate system (*1*). The Walker circulation is a critical component of the tropical climate system and is closely tied to zonal coupled ocean-atmospheric modes, such as the Indian Ocean dipole (IOD), but its response to global warming is still debated (*2*, *3*). Some studies predict a weakening Walker circulation due to different rates of increasing precipitation and moisture under greenhouse warming (*3*), leading to more frequent extreme IOD events (*4*), whereas other studies suggest no detectable changes in IOD (*5*). Whereas these studies emphasize the impacts of radiative forcing in the tropics on the Walker circulation, the weakening Atlantic meridional overturning circulation (AMOC) due to increased greenhouse gases (GHG) (*6*) and freshwater discharge from Greenland ice sheet and Arctic sea ice melting (*7*, *8*) is also predicted to exert a remote influence on the Walker circulation (*9*, *10*). Therefore, understanding the influence of North Atlantic climate perturbations on the Walker circulation is particularly important for climate prediction.

Millennial-scale North Atlantic cooling events during the last deglaciation caused by meltwater/iceberg discharge [e.g., Heinrich Stadial 1 (HS1), ~18 to 14.5 thousand years (ka) ago; and Younger Dryas (YD), ~12.9 to 11.7 ka ago] have long been used to investigate global responses to AMOC perturbations and provide a unique opportunity to investigate the tropical response to North Atlantic forcing under different boundary conditions (*11*–*19*). Previous modeling and proxy studies of HS1 and YD have focused on interhemispherically antiphased precipitation changes in the tropics attributed to meridional shifts of the intertropical convergence zone (ITCZ) (*11*, *13*, *14*). Although meridional precipitation anomalies are recorded from the Atlantic (*15*, *16*) and South America (*18*, *20*, *21*) during HS1, proxy records show complex spatial patterns in other regions. These include interhemispheric drought extending from northern Africa to southern tropical Africa (~20°S) (Fig. 1) and heterogeneous precipitation patterns over the Maritime Continent (*17*, *19*, *22*). These records suggest that ITCZ displacement alone does not fully explain precipitation anomalies in the tropics during Heinrich events, but to date, there is no alternative theory to explain variations in the tropical Indian Ocean (IO) region. Here, we explore the mechanisms of hydroclimate changes over the tropical IO during HS1 by integrating a new isotope-enabled transient climate model experiment (iTRACE) (*23*) and multiproxy hydroclimate records across the IO.

RESULTS

Proxy model synthesis

We used iTRACE (*23*) to investigate the mechanisms driving hydroclimate changes over the IO during HS1 inferred from proxy data and their imprint on water isotopes (Materials and Methods). iTRACE was performed from the Last Glacial Maximum (LGM) to the early Holocene (20 to 11 ka ago) using the water isotope-enabled Community Earth System Model 1.3 (iCESM1.3). iCESM is capable of simulating major features of water isotopes and climate variations during the last deglaciation, including the IO region (*23*–

[1]Department of Earth, Environmental, and Planetary Sciences, Brown University, Providence, RI, USA. [2]Institute at Brown for Environment and Society, Brown University, Providence, RI, USA. [3]Atmospheric Science Program, Department of Geography, The Ohio State University, Columbus, OH, USA. [4]Climate and Global Dynamics Laboratory, National Center for Atmospheric Research, Boulder, CO, USA. [5]Geology and Geophysics Department, Woods Hole Oceanographic Institution, Woods Hole, MA, USA. [6]MARUM-Center for Marine Environmental Sciences, University of Bremen, Bremen, Germany. [7]Frontier Science Center for Deep Ocean Multispheres and Earth System (FDOMES) and Physical Oceanography Laboratory, Ocean University of China, Qingdao, China. [8]Department of Marine Chemistry and Geochemistry, Woods Hole Oceanographic Institution, Woods Hole, MA, USA. [9]State Key Laboratory of Isotope Geochemistry, CAS Center for Excellence in Deep Earth Science, Guangzhou Institute of Geochemistry, Chinese Academy of Sciences, Guangzhou, China. [10]Department of Marine and Coastal Sciences and Department of Earth and Planetary Sciences, Rutgers, State University of New Jersey, New Brunswick, NJ, USA. [11]Department of Surface Waters Research and Management, Eawag, Dübendorf, Switzerland. [12]Department of Earth Sciences, ETH Zürich, Zürich, Switzerland. [13]Department of Atmospheric and Oceanic Sciences, School of Physics, Peking University, Beijing, China.
*Corresponding author. Email: xiaojing_du@brown.edu

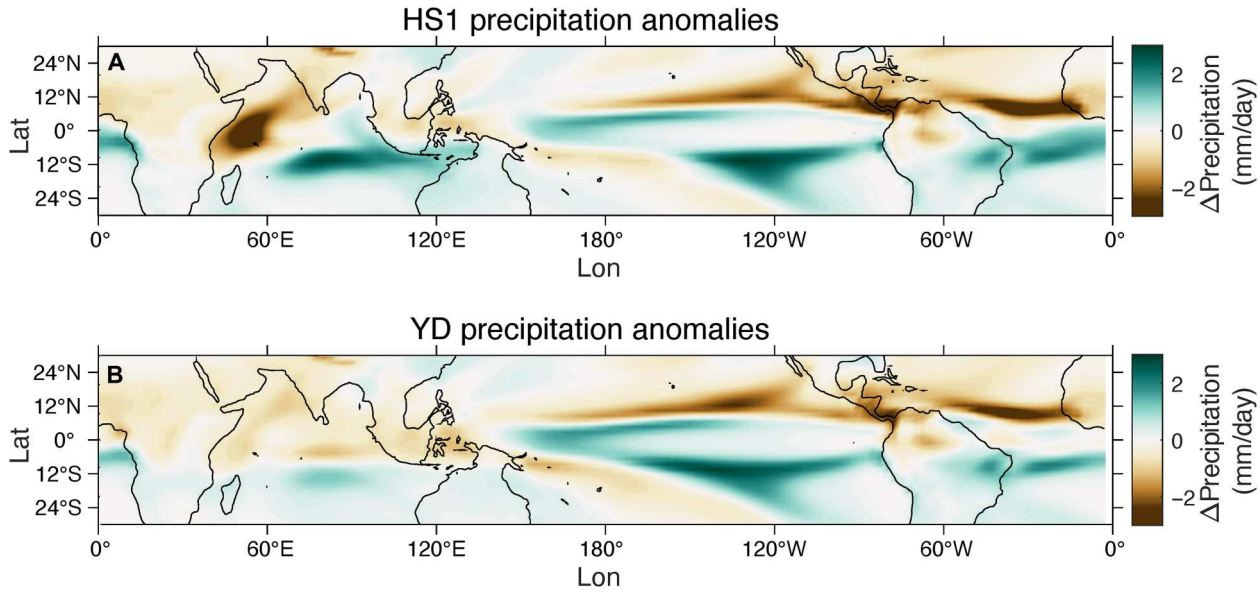

Fig. 1. Simulated precipitation anomalies across the tropical domain. (**A**) HS1 (14.5 to 18 ka ago) and (**B**) YD (11.7 to 12.9 ka ago) relative to the Bølling-Allerød (BA, 12.9 to 14.5 ka ago) in response to meltwater flux (MWF) in iTRACE. Coastlines (black outline) for HS1 and YD correspond to 120- and 60-m drop in sea level, respectively.

25). Comparison with modern observations also suggests that iCESM can realistically capture the observed spatial pattern of precipitation and $\delta^{18}O_{precip}$ anomalies associated with the IO zonal mode (fig. S1). In iTRACE, four simulations with four realistic forcing scenarios were applied additively, including ice sheet and ocean bathymetry (ICE), insolation (ICE + ORB), GHG (ICE + ORB + GHG), and full-forcing including meltwater fluxes (MWFs) (ICE + ORB + GHG + MWF). The effects of MWFs were isolated by subtracting ICE + ORB + GHG from the full-forcing experiment to investigate the tropical response to North Atlantic forcing.

We compiled multiproxy hydroclimate records spanning the deglaciation from across the IO and compared these records to the outputs from iTRACE. We synthesized precipitation-sensitive proxies from the Maritime Continent and East Africa, as well as proxy data reflecting sea surface temperature (SST) and thermocline depth in the tropical IO. Our synthesis resulted in a network of 24 precipitation (table S1), 33 SST (table S2), and 5 thermocline depth proxy records (table S3). The precipitation data include speleothem $\delta^{18}O$, leaf wax δD, lake level, pollen, and detrital sediment flux. We classified precipitation anomalies as either drier or wetter as these proxies do not provide a quantitative estimate of precipitation change. To facilitate comparison to meltwater-forcing simulations in iTRACE, we normalized and detrended SST data (Mg/Ca of planktic foraminifera or U^K_{37} index) to remove the deglacial warming trend. The relative depth of the thermocline was inferred from the difference between surface and thermocline temperatures (larger difference indicates shallower thermocline and vice versa). Both HS1 (14.5 to 18 ka ago) and YD (11.7 to 12.9 ka ago) hydroclimate anomalies were calculated relative to the Bølling-Allerød (BA, 12.9 to 14.5 ka ago), which serves as a baseline for the comparison to assess responses to AMOC and expand the proxy network (some records do not extend to LGM).

The MWF simulation predicts a large east-west precipitation dipole anomaly over the tropical IO during HS1. This dipole is unique to the IO and to HS1 and emerges in the context of north-south dipole anomalies in precipitation simulated elsewhere in the tropics during HS1 and over the tropical IO during the YD (Fig. 1 and fig. S6). Widespread drying was simulated in the western IO, from the Arabian Sea and northern Africa to ~15°S south of the equator, whereas wetter conditions dominate from the central equatorial to the eastern and southern Maritime Continent (Fig. 2). Precipitation reconstructions indicate widespread drying in tropical East Africa (from northern Africa to ~20°S) during HS1 and a more heterogeneous pattern in the Maritime Continent, including wetter conditions in Java and Flores, little change or dry over Sumatra, weak drying to no change on Sulawesi (*26*, *27*), and dry conditions in northern Borneo, similar to the simulations (Fig. 2). Simulated SST anomalies in response to MWF also display a zonal dipole over the tropical IO with warming in the eastern IO and moderate cooling over the west (Fig. 2). The precipitation dipole in the proxy reconstructions, with drying in the west and generally wetter (but more heterogeneous) conditions in the east, shows statistically significant agreement with the simulations, with a Cohen's $\kappa = 0.71$ ($P < 0.01$). The SST change in proxy reconstructions and simulations are also correlated [correlation coefficient (r) = 0.56, $P < 0.01$], and both proxy records and simulations show that the thermocline deepened over the eastern IO and shoaled over the western IO during HS1.

IO zonal dipole in response to HS1

The zonal dipole in precipitation, SST, and thermocline depth suggests a strengthened IO Walker circulation during HS1. This is consistent with decreased ascending motion and convection in the western IO and increased ascending motion and convection over the eastern IO indicated by vertical velocity anomalies (Fig. 3C). This dipole arises because of interactions between the North Atlantic heat transport, the ITCZ, and the IO Walker circulation. The southward shift of the ITCZ in response to abrupt AMOC reductions and North Atlantic cooling during HS1 reduces precipitation

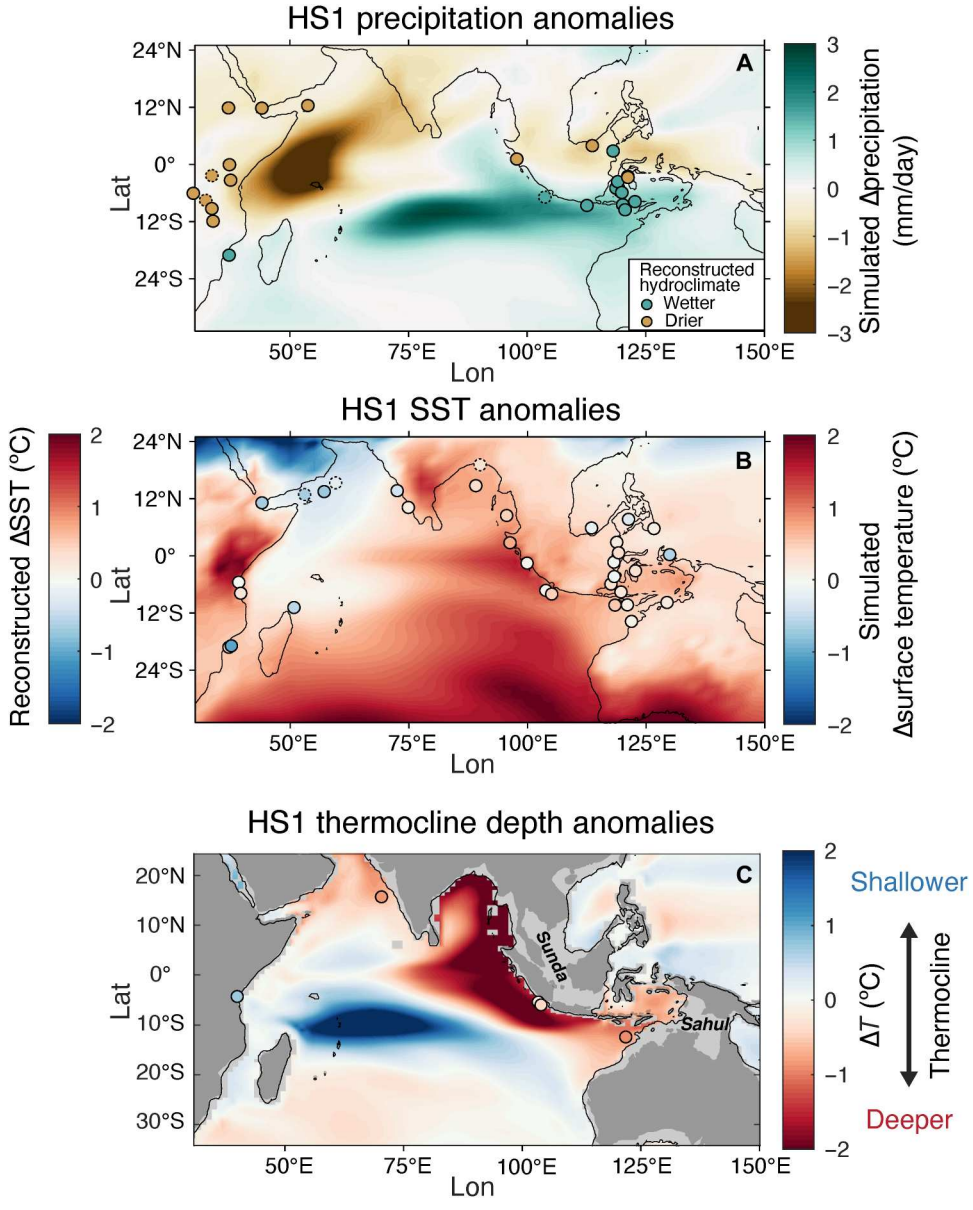

Fig. 2. Proxy-model synthesis over the tropical IO. Changes in (**A**) precipitation, (**B**) surface temperature, and (**C**) thermocline depth during HS1 relative to BA in response to MWF in iTRACE. The network of precipitation-sensitive proxies includes speleothem $\delta^{18}O$, leaf wax δD, detrital flux, pollen, and lake level, capturing drier (brown) or wetter (green) conditions at HS1. All speleothem $\delta^{18}O$ and leaf wax δD values have been corrected for global ice volume effects on the isotopic composition of seawater. SSTs derived from Mg/Ca of planktonic foraminifera and $U^{K'}_{37}$ index were normalized and detrended to remove the deglacial warming trend when calculating the HS1 SST anomalies. The changes in thermocline depth were inferred from the difference between SST and the temperature of thermocline depth (75 m) in model simulation, and difference between the Mg/Ca-based temperatures of surface- and thermocline-dweller planktic foraminifera species. Dashed circles represent sites where HS1 anomalies records are less robust because of chronologic uncertainties or low temporal resolution (see Materials and Methods for details). The HS1 coastlines estimated from modern bathymetry at 120 m below sea level today are indicated by the black outline in (C). The HS1 land-sea configuration in iTRACE (light gray shadow), modern land mask (dark gray shadow), and the location of Sunda and Sahul shelves are also shown in (C).

in the Northern Hemisphere (NH) tropics and promotes precipitation in the Southern Hemisphere (SH) tropics, as observed in the Pacific and Atlantic Ocean basins (Fig. 1A). Over the IO, the strengthened Hadley cell and trade winds in NH (*28*–*30*) during HS1 produce northeasterly wind anomalies and cooling over the Arabian Sea (Fig. 3B). The weakened SH Hadley cell leads to weakened southeasterly trade winds in the equatorial eastern IO (indicated by northwesterly anomalies in Fig. 3B), which suppress the upwelling of cooler water off Sumatra and Java, deepen the thermocline (fig. S2), and warm SST over this region. Such SST anomalies strengthen the IO Walker circulation via the Bjerknes feedback (*31*), leading to wetter/warmer conditions and a deeper thermocline in the eastern IO and the opposite response in the western IO.

The weakened southeasterly trade winds in the equatorial eastern IO arising from ITCZ migration thus promote mean conditions during HS1 that resemble the negative phase of the modern-

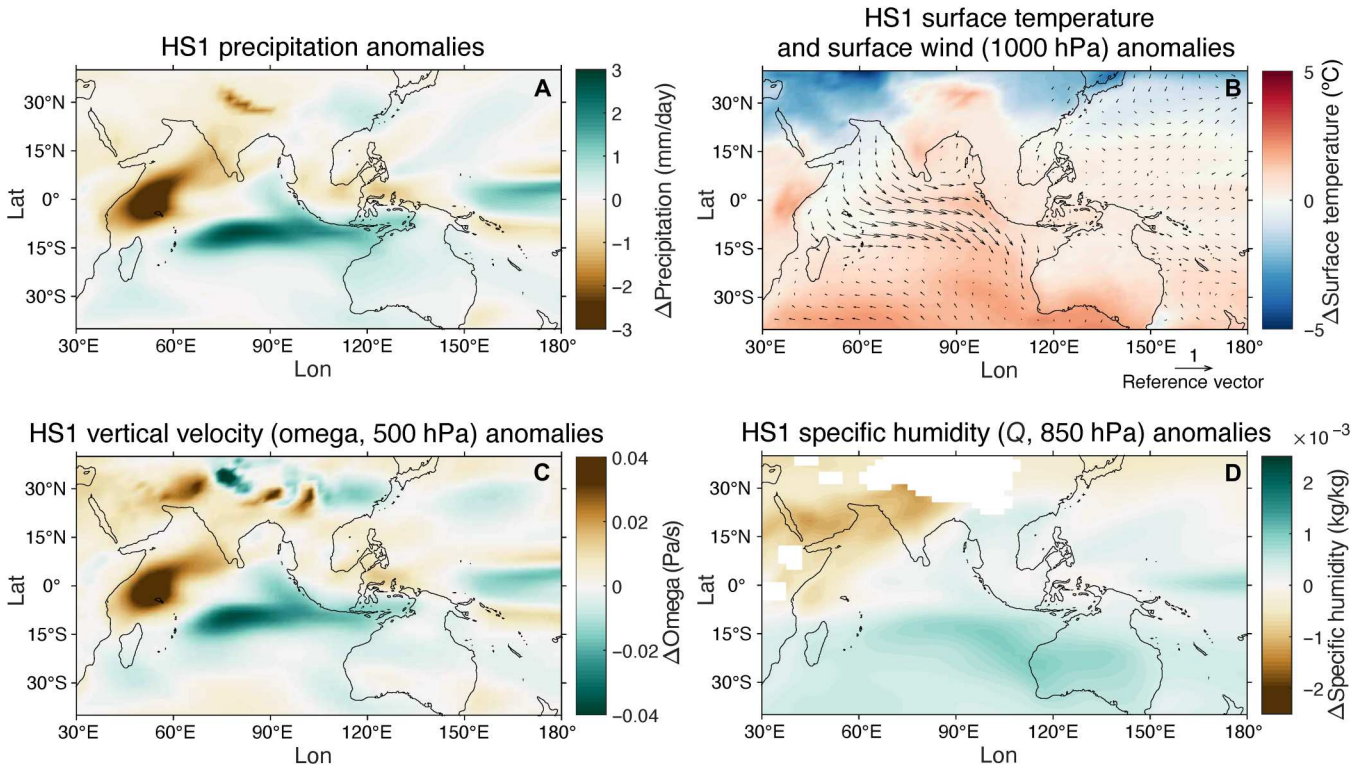

Fig. 3. Simulated climate anomalies over the tropical IO. Changes in (**A**) precipitation, (**B**) surface temperature and surface wind at 1000-hPa level, (**C**) vertical velocity (omega) at 500-hPa level, and (**D**) specific humidity (*Q*) at 850-hPa level during HS1 relative to BA in response to MWF in iTRACE. The HS1 coastlines (black outline) correspond to a 120-m drop in sea level.

day IOD. The zonal dipole anomalies in winds and temperature strengthen in boreal summer and peak in boreal fall (figs. S3 and S4), similar to modern IOD events. Determining the relationships between seasonal-to-interannual variability and the millennial-scale mean state during HS1 would require further analysis; however, we note that interannual surface temperature variability west of the Maritime Continent increased during HS1, relative to the YD in iTRACE (fig. S5) and similar to previous studies (*32*, *33*). The probability density functions of the simulated IOD index in iTRACE also suggest a higher probability of negative IOD events during HS1 (fig. S6). This shift could contribute to the long-term zonal dipole and strengthened Walker circulation during HS1 in the IO.

The zonal dipole is unique to HS1 and the IO, standing in contrast to the meridional dipole structure that develops in the tropical IO during the YD (Fig. 1B and fig. S7) and in other tropical oceans during HS1 (Fig. 1A). The amplitude of AMOC decline in iTRACE is comparable during HS1 and YD, but the zonal responses are distinct to HS1, implying that AMOC alone cannot explain the IO zonal dipole (fig. S10). Similarly, the proxy network indicates distinct YD and HS1 responses that align with meridional shifts during the YD and zonal changes during HS1 (Fig. 3 and fig. S7). We suggest that the zonal IO response arises from the impact of lower sea level and exposed continental shelves in the Maritime Continent during HS1. Previous model and proxy studies indicate that during the LGM, the exposure of the Sunda and Sahul shelves induces a positive Bjerknes feedback and a weak Walker circulation across the IO, causing drying over the eastern IO and wetter conditions in coastal East Africa (*34*–*36*)—the opposite conditions from those that we observe during HS1. The strengthening of the IO Walker circulation in response to HS1 thus opposes the preexisting weaker Walker circulation during the LGM (fig. S8), amplifying the magnitude of the zonal dipole anomalies over the IO (we note that HS1 anomalies calculated relative to LGM are very similar to anomalies relative to BA in iTRACE; fig. S9). The Sunda and Sahul shelves remained largely exposed during HS1 [both in our simulations (*24*) and according to sea level reconstructions applied to the current bathymetry] but were partially inundated during the YD (Fig. 1). In particular, between HS1 and YD, the rising sea levels inundated the northwest (NW) Australia shelf and parts of the Sunda shelf, both of which have been shown to be important to zonal circulation over the IO (*24*, *33*), explaining the different responses to MWF during these intervals. This highlights the sensitivity and complexity of the IO climate and its response to different global boundary conditions.

Megadroughts and extreme precipitation across the IO

The IO zonal dipole triggered hydrological extremes across the basin, including widespread droughts in East Africa and increased precipitation over most of Indonesia. It has long been a challenge to explain the zonal asymmetric hydroclimate anomalies during HS1 over the tropical IO. Previous studies attributed droughts in East Africa during HS1 to an extreme shift of the ITCZ to southernmost Africa (*37*, *38*), a weakening of Indian winter monsoon circulation (*39*), and/or weakened moisture advection due to lower northwestern IO SSTs (*12*, *40*, *41*). Although the MWF simulation in iTRACE

supports an instantaneous cooling of the surface Arabian Sea and reduced southerly monsoon wind strength during HS1, the reduced specific humidity (Fig. 3D) associated with cooling SSTs (Fig. 3B) over western IO only leads to moderately dry conditions in equatorial and northeast Africa. Our results suggest that the strengthened IO Walker circulation during HS1 and the consequent reduction in convection over the western IO are responsible for widespread droughts in this region (Fig. 3A), such as droughts recorded from Lake Malawi (*39*), Lake Tanganyika (*40*), and the complete desiccation of Lake Victoria (*42*).

Previous studies have also debated the spatially heterogeneous precipitation anomalies over the Maritime Continent, particularly near and north of the equator (*17*, *22*, *27*, *43*). Our results suggest that stronger ascending motion and convection over the eastern IO due to the anomalously strong Walker circulation were superimposed on a north-south dipole structure caused by southward migration of the ITCZ during HS1 (Fig. 3). These processes could interact constructively to intensify wet conditions in the southern Maritime Continent while creating negative interactions that weaken or eliminate anomalies in the northern tropics, such as Sumatra, leading to a spatially heterogeneous response to HS1 over the Maritime Continent. Weak responses to HS1 were reported in hydrological reconstructions from the coast of Sumatra and Sulawesi (*44*, *45*), whereas dry conditions were inferred from stalagmite $\delta^{18}O$ in northern Borneo (*17*). On the other hand, multiproxy records from Flores Sea (*19*), Flores (*43*), and East Java (*46*) indicate substantially higher precipitation during HS1.

Implications for the large-scale water cycle

Although the HS1 dipole is centered over the IO, it has remote effects on more distal regions, such as the Asian summer monsoon domain. Water isotope–based records throughout Asia are often interpreted to reflect local precipitation amount and the intensity of the Asian summer monsoon (*47*, *48*); however, more recent studies suggested that these records more likely reflect nonlocal processes, such as changes in the $\delta^{18}O$ of water vapor ($\delta^{18}O_{vapor}$) in moisture source regions (*23*, *49*, *50*). Previous water tagging experiments using iCESM demonstrate that water vapor over the Asian monsoon region originates mainly from the IO (*23*), where the IO zonal dipole caused widespread $\delta^{18}O_{precip}$ enrichment during HS1. Our simulation results show that the enriched $\delta^{18}O_{vapor}$ from the western IO is advected into the Asian monsoon region where it contributes to widespread $\delta^{18}O_{precip}$ anomalies during HS1 (Fig. 4A and fig. S11A), consistent with previous water tagging experiments (*23*). In addition, reduced precipitation over the Indian subcontinent and southern Asian monsoon region could further intensify the $\delta^{18}O_{precip}$ enrichment (*23*, *49*). Both our simulations and proxy data (*23*) show relatively modest enrichment of $\delta^{18}O_{precip}$ in Asian monsoon regions during the YD (*23*) relative to HS1 (Fig. 4B), indicating that the equatorial IO zonal dynamics are essential to $\delta^{18}O_{precip}$ in this region.

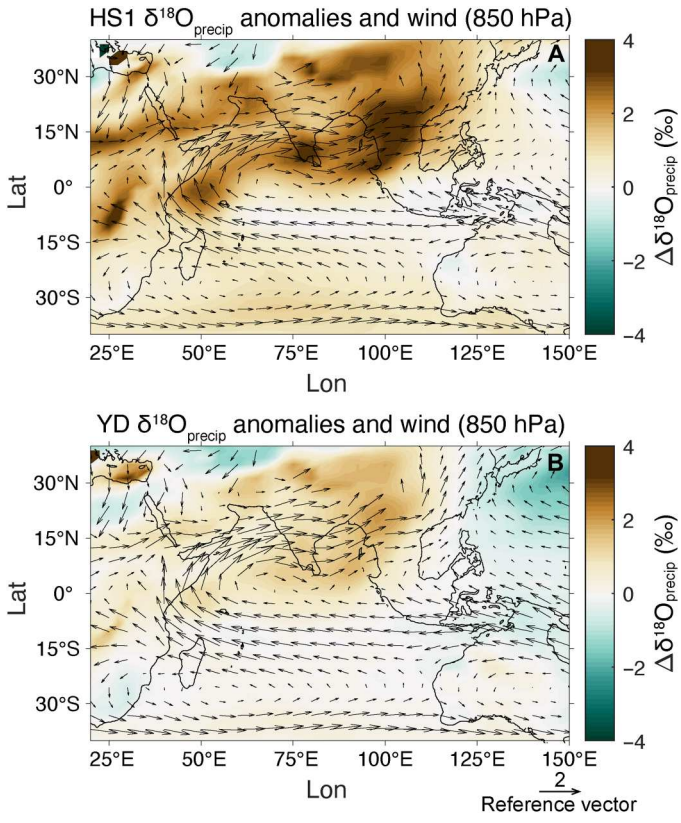

Fig. 4. Simulated summer (June to August) $\delta^{18}O_{precip}$ anomalies and wind (850 hPa). (**A**) HS1 and (**B**) YD relative to BA in response to MWF in iTRACE. The wind field in (A) and (B) represent mean conditions during HS1 and YD, respectively. Coastlines (black outline) for HS1 and YD correspond to 120- and 60-m drop in sea level, respectively.

DISCUSSION

Our study suggests that an east-west precipitation dipole developed over the tropical IO during HS1 as a result of a north-south displacement of the ITCZ. The southward ITCZ shift over the eastern IO during HS1 suppresses upwelling of cooler water off Sumatra and Java. The consequent warmer SST in this region strengthens IO Walker circulation via the Bjerknes feedback, triggering an east-west precipitation dipole across the basin. This zonal precipitation dipole triggers hydrological extremes across the tropical IO, including widespread droughts in East Africa and increased precipitation over most of Indonesia. In addition, the enriched $\delta^{18}O_{precip}$ over western IO caused by the IO zonal dipole has a remote effect on Asian summer monsoon domain and contribute to widespread $\delta^{18}O_{precip}$ anomalies in this region during HS1.

Although neither exposure of continental shelves nor AMOC shutdown from ice sheet discharge are directly analogous to future climate warming scenarios, the impacts of these forcings on coupled ocean-atmosphere interactions over the IO highlights the sensitivity of zonal asymmetries and their importance to future changes in tropical precipitation patterns. Historical observations and model predictions suggest that increasing atmospheric GHG will cause the IO thermocline to shoal and intensify the ocean-atmosphere feedbacks across the tropical IO, analogous to the glacial background climate state (*24*, *33*–*35*). The potential for reduced AMOC under global warming suggests the possibility of complex and unpredictable changes in IO zonal circulation and precipitation, as changes in the AMOC could mitigate or exacerbate the impacts of warming.

MATERIALS AND METHODS

Climate model experiments

We compared a multiproxy synthesis with simulated hydroclimate changes in iTRACE, which is the first transient simulation of the global and water isotopes evolution during the last deglaciation (*23*). Conducted with iCESM1.3 (*51*), iTRACE is composed of the Community Atmosphere Model (CAM5.3), the Community Land Model (CLM4), Parallel Ocean Program (POP2), and Los Alamos Sea Ice Model (CICE4). The simulations in iTRACE start from the LGM (20 ka ago) and end at the early Holocene (11 ka ago). Four forcings, including ice sheet and ocean bathymetry, insolation, GHG, and MWF, were applied additively, allowing the estimation of single forcing effect by comparing different simulations. Specifically, the baseline simulation is integrated with changing ice sheets and ocean bathymetry (ICE), before orbital forcings was additively introduced (ICE + ORB), which is followed by GHG (ICE + ORB + GHG). MWF were added to generate a full forcing simulation (ICE + ORB + GHG + MWF).

In iTRACE, the continental ice sheet configuration is based on the ICE-6G model (*52*) and was modified every 1000 years; GHG concentrations (CO_2, CH_4, and N_2O) were prescribed following ice core reconstructions (*53*–*55*); the MWF follows the scheme used in TRACE-21 (*56*), which is approximately consistent with sea level reconstructions. The global ice history model ICE-6G is based on realistic geological and geodetic observations. The sea level boundary conditions and ocean bathymetry was estimated by applying the global sea level changes according to ICE-6G model to the present-day seafloor topography and was changed at 14 and 12 ka ago. Specifically, the LGM land-sea configuration lasts until 14 ka ago, after which the NW Australia shelf and parts of Sunda shelf were inundated (the Sunda and Sahul shelves coastline corresponds to the −75-m preindustrial isobath), and the bathymetry of the North Sea, Barents Sea, and Kara Sea were restored to the preindustrial conditions. At 12 ka ago, the main body of the Sunda and Sahul shelves were inundated, and the Bering Strait was partly opened.

The precipitation and water isotope simulations of iCESM have been validated against instrument observations at global scale (*51*). To further evaluate the performance of iCESM in the IO domain, we compared the iCESM simulations (1850 to 2005) (*51*, *57*) with monthly precipitation data (1979 to 2020) from the Global Precipitation Climatology Project (*58*) (https://psl.noaa.gov/data/gridded/data.gpcp.html), and monthly $\delta^{18}O_{precip}$ data (1962 to 2016) spanning at least 8 years from the Global Network of Isotopes in Precipitation (GNIP; https://iaea.org/services/networks/gnip). Both observed and simulated precipitation and $\delta^{18}O_{precip}$ anomalies when comparing negative and positive IOD months (IOD index above 0.4 or below −0.4, respectively) show zonal dipole across the tropical IO. Wetter conditions were observed over central and eastern IO and throughout the Maritime Continent, especially the southern Sumatra and east Java, whereas widespread drying dominated the western IO and eastern Africa. Simulated IOD related $\delta^{18}O_{precip}$ anomalies largely resemble observations in East Africa and the Maritime Continent, although the simulated southward extension of $\delta^{18}O_{precip}$ enrichment in the eastern Africa is less than that in the GNIP data.

Proxy synthesis

We synthesized well-dated proxy records that have sufficient resolution to observe HS1-BA precipitation and SST anomalies from the Maritime Continent and East Africa. All SST proxy records (Mg/Ca of planktic foraminifera or U^K_{37} index) were normalized and detrended by removing the linear trend in each record to remove the deglacial warming trend before calculating the HS1 SST anomalies. The age models of all proxy records are based on accelerated mass spectrometry (AMS) radiocarbon dates, except for core TY93929/P, GeoB3007-1, and SO93-126 K, whose chronologies are based on oxygen isotope stratigraphy. For consistency, we recalibrated all age models of marine/terrestrial sediment records with radiocarbon chronology using the Marine20 (*59*) / IntCal20 (*60*) radiocarbon calibration curve with the BACON age model program (*61*), except for core AAS9-21, Lake Challa, Lake Rukwa, Lake Victoria, and core MD98-2152. For marine sediments records, ΔR was determined as the weighted average of ΔR near each site from http://calib.org/marine/. We use the published age models for core AAS9-21 and Lake Challa as their AMS radiocarbon dates are not publicly available. For Lake Rukwa and Lake Victoria, the HS1 precipitation anomalies are inferred from the interpretation in previous literature (*62*, *63*). The δD_{wax} record from core MD98-2152 only contains one data point during BA. Core MD98-2152, Lake Rukwa, and Lake Victoria are therefore not included in the Cohen's κ analysis.

Supplementary Materials

This PDF file includes:

Figs. S1 to S13
Tables S1 to S3
References

REFERENCES AND NOTES

1. G. R. McGregor, S. Nieuwolt, *Tropical Climatology: An Introduction to the Climates of the Low Latitudes* (John Wiley & Sons Ltd, ed. 2, 1998).
2. A. C. Clement, R. Seager, M. A. Cane, S. E. Zebiak, An ocean dynamical thermostat. *J. Climate* **9**, 2190–2196 (1996).
3. G. A. Vecchi, B. J. Soden, A. T. Wittenberg, I. M. Held, A. Leetmaa, M. J. Harrison, Weakening of tropical Pacific atmospheric circulation due to anthropogenic forcing. *Nature* **441**, 73–76 (2006).
4. W. Cai, A. Santoso, G. Wang, E. Weller, L. Wu, K. Ashok, Y. Masumoto, T. Yamagata, Increased frequency of extreme Indian Ocean dipole events due to greenhouse warming. *Nature* **510**, 254–258 (2014).
5. X.-T. Zheng, S.-P. Xie, Y. Du, L. Liu, G. Huang, Q. Liu, Indian Ocean dipole response to global warming in the CMIP5 multimodel ensemble. *J. Climate* **26**, 6067–6080 (2013).
6. L. Muntjewerf, M. Petrini, M. Vizcaino, C. Ernani da Silva, R. Sellevold, M. D. W. Scherrenberg, K. Thayer-Calder, S. L. Bradley, J. T. M. Lenaerts, W. H. Lipscomb, M. Lofverstrom, Greenland ice sheet contribution to 21st century sea level rise as simulated by the coupled CESM2.1-CISM2.1. *Geophys. Res. Lett.* **47**, e2019GL086836 (2020).
7. E. Hanna, P. Huybrechts, K. Steffen, J. Cappelen, R. Huff, C. Shuman, T. Irvine-Fynn, S. Wise, M. Griffiths, Increased runoff from melt from the Greenland Ice Sheet: A response to global warming. *J. Climate* **21**, 331–341 (2008).
8. W. Jiang, G. Gastineau, F. Codron, Multicentennial variability driven by salinity exchanges between the atlantic and the arctic ocean in a coupled climate model. *J. Adv. Model. Earth Syst.* **13**, e2020MS002366 (2021).
9. A. Timmermann, Y. Okumura, S.-I. An, A. Clement, B. Dong, E. Guilyardi, A. Hu, J. Jungclaus, M. Renold, T. F. Stocker, The influence of a weakening of the Atlantic meridional overturning circulation on ENSO. *J. Climate* **20**, 4899–4919 (2007).
10. B. Dong, R. T. Sutton, Enhancement of ENSO variability by a weakened atlantic thermohaline circulation in a coupled GCM. *J. Climate* **20**, 4920–4939 (2007).
11. M. Mohtadi, M. Prange, D. W. Oppo, R. De Pol-Holz, U. Merkel, X. Zhang, S. Steinke, A. Luckge, North Atlantic forcing of tropical Indian Ocean climate. *Nature* **509**, 76–80 (2014).

12. J. C. Stager, D. B. Ryves, B. M. Chase, F. S. Pausata, Catastrophic drought in the Afro-Asian monsoon region during Heinrich event 1. *Science* **331**, 1299–1302 (2011).
13. E. Schefuss, H. Kuhlmann, G. Mollenhauer, M. Prange, J. Patzold, Forcing of wet phases in southeast Africa over the past 17,000 years. *Nature* **480**, 509–512 (2011).
14. D. McGee, A. Donohoe, J. Marshall, D. Ferreira, Changes in ITCZ location and cross-equatorial heat transport at the last glacial maximum, Heinrich stadial 1, and the mid-Holocene. *Earth Planet. Sci. Lett.* **390**, 69–79 (2014).
15. G. Deplazes, A. Lückge, L. C. Peterson, A. Timmermann, Y. Hamann, K. A. Hughen, U. Röhl, C. Laj, M. A. Cane, D. M. Sigman, G. H. Haug, Links between tropical rainfall and North Atlantic climate during the last glacial period. *Nat. Geosci.* **6**, 213–217 (2013).
16. L. C. Peterson, G. H. Haug, K. A. Hughen, U. Röhl, Rapid changes in the hydrologic cycle of the tropical atlantic during the last glacial. *Science* **290**, 1947–1951 (2000).
17. J. W. Partin, K. M. Cobb, J. F. Adkins, B. Clark, D. P. Fernandez, Millennial-scale trends in west Pacific warm pool hydrology since the last glacial maximum. *Nature* **449**, 452–453 (2007).
18. P. A. Baker, S. C. Fritz, Nature and causes of Quaternary climate variation of tropical South America. *Quat. Sci. Rev.* **124**, 31–47 (2015).
19. J. Muller, J. F. McManus, D. W. Oppo, R. Francois, Strengthening of the Northeast Monsoon over the Flores Sea, Indonesia, at the time of Heinrich event 1. *Geology* **40**, 635–638 (2012).
20. X. Wang, A. S. Auler, R. L. Edwards, H. Cheng, P. S. Cristalli, P. L. Smart, D. A. Richards, C.-C. Shen, Wet periods in northeastern Brazil over the past 210 kyr linked to distant climate anomalies. *Nature* **432**, 740–743 (2004).
21. P. A. Baker, S. C. Fritz, S. J. Burns, E. Ekdahl, C. A. Rigsby, The nature and origin of decadal to millennial scale climate variability in the southern tropics of South America: The Holocene record of Lago Umayo, Peru, in *Past Climate Variability in South America and Surrounding Regions,* F. Vimeux, F. Sylvestre, M. Khodri, Eds.(Springer, 2009), pp. 301–322.
22. E. M. Niedermeyer, A. L. Sessions, S. J. Feakins, M. Mohtadi, Hydroclimate of the western Indo-Pacific warm pool during the past 24,000 years. *Proc. Natl. Acad. Sci. U.S.A.* **111**, 9402–9406 (2014).
23. C. He, Z. Liu, B. L. Otto-Bliesner, E. C. Brady, C. Zhu, R. Tomas, P. U. Clark, J. Zhu, A. Jahn, S. Gu, J. Zhang, J. Nusbaumer, D. Noone, H. Cheng, Y. Wang, M. Yan, Y. Bao, Hydroclimate footprint of pan-Asian monsoon water isotope during the last deglaciation. *Sci. Adv.* **7**, eabe2611 (2021).
24. X. Du, J. M. Russell, Z. Liu, B. L. Otto-Bliesner, Y. Gao, C. Zhu, D. W. Oppo, M. Mohtadi, Y. Yan, V. V. Galy, C. He, Deglacial trends in Indo-Pacific warm pool hydroclimate in an isotope-enabled Earth system model and implications for isotope-based paleoclimate reconstructions. *Quat. Sci. Rev.* **270**, 107188 (2021).
25. C. He, Z. Liu, L. Otto-Bliesner Bette, C. Brady Esther, C. Zhu, R. Tomas, C. Buizert, P. Severinghaus Jeffrey, Abrupt Heinrich Stadial 1 cooling missing in Greenland oxygen isotopes. *Sci. Adv.* **7**, eabh1007
26. J. M. Russell, H. Vogel, B. L. Konecky, S. Bijaksana, Y. S. Huang, M. Melles, N. Wattrus, K. Costa, J. W. King, Glacial forcing of central Indonesian hydroclimate since 60,000 y B.P. *Proc. Natl. Acad. Sci. U.S.A.* **111**, 5100–5105 (2014).
27. C. E. Krause, M. K. Gagan, G. B. Dunbar, W. S. Hantoro, J. C. Hellstrom, H. Cheng, R. L. Edwards, B. W. Suwargadi, N. J. Abram, H. Rifai, Spatio-temporal evolution of Australasian monsoon hydroclimate over the last 40,000 years. *Earth Planet. Sci. Lett.* **513**, 103–112 (2019).
28. D. Mcgee, E. Moreno-Chamarro, B. Green, J. Marshall, E. Galbraith, L. Bradtmiller, Hemispherically asymmetric trade wind changes as signatures of past ITCZ shifts. *Quat. Sci. Rev.* **180**, 214–228 (2018).
29. J. C. H. Chiang, A. R. Friedman, Extratropical cooling, interhemispheric thermal gradients, and tropical climate change. *Annu. Rev. Earth Planet. Sci.* **40**, 383–412 (2012).
30. I. Cvijanovic, J. C. H. Chiang, Global energy budget changes to high latitude North Atlantic cooling and the tropical ITCZ response. *Climate Dynam.* **40**, 1435–1452 (2013).
31. J. Bjerknes, Atmospheric teleconnections from the equatorial PACIFIC1. *Mon. Weather Rev.* **97**, 163–172 (1969).
32. K. Thirumalai, P. N. DiNezio, J. E. Tierney, M. Puy, M. Mohtadi, An El Niño mode in the Glacial Indian Ocean? *Paleoceanogr. Paleoclimatol.* **34**, 1316–1327 (2019).
33. P. N. DiNezio, M. Puy, K. Thirumalai, F.-F. Jin, J. E. Tierney, Emergence of an equatorial mode of climate variability in the Indian Ocean. *Sci. Adv.* **6**, eaay7684 (2020).
34. P. N. DiNezio, J. E. Tierney, The effect of sea level on glacial Indo-Pacific climate. *Nat. Geosci.* **6**, 485–491 (2013).
35. P. N. DiNezio, J. E. Tierney, B. L. Otto-Bliesner, A. Timmermann, T. Bhattacharya, N. Rosenbloom, E. Brady, Glacial changes in tropical climate amplified by the Indian Ocean. *Sci. Adv.* **4**, eaat9658 (2018).
36. P. N. Di Nezio, A. Timmermann, J. E. Tierney, F.-F. Jin, B. Otto-Bliesner, N. Rosenbloom, B. Mapes, R. Neale, R. F. Ivanovic, A. Montenegro, The climate response of the Indo-Pacific warm pool to glacial sea level. *Paleoceanography* **31**, 866–894 (2016).
37. D. Verschuren, J. S. S. Damste, J. Moernaut, I. Kristen, M. Blaauw, M. Fagot, G. H. Haug; CHALLACEA project members, Half-precessional dynamics of monsoon rainfall near the East African equator. *Nature* **462**, 637–641 (2009).
38. I. S. Castañeda, J. P. Werne, T. C. Johnson, Wet and arid phases in the southeast African tropics since the last glacial maximum. *Geology* **35**, 823–826 (2007).
39. B. L. Konecky, J. M. Russell, T. C. Johnson, E. T. Brown, M. A. Berke, J. P. Werne, Y. Huang, Atmospheric circulation patterns during late Pleistocene climate changes at Lake Malawi, Africa. *Earth Planet. Sci. Lett.* **312**, 318–326 (2011).
40. J. E. Tierney, J. M. Russell, Y. S. Huang, J. S. S. Damste, E. C. Hopmans, A. S. Cohen, Northern hemisphere controls on tropical southeast African climate during the past 60,000 years. *Science* **322**, 252–255 (2008).
41. J. E. Tierney, F. S. R. Pausata, P. DeMenocal, Deglacial Indian monsoon failure and North Atlantic stadials linked by Indian Ocean surface cooling. *Nat. Geosci.* **9**, 46–50 (2016).
42. C. Johnson Thomas, A. Scholz Christopher, R. Talbot Michael, K. Kelts, R. D. Ricketts, G. Ngobi, K. Beuning, I. Ssemmanda, J. W. McGill, Late pleistocene desiccation of lake victoria and rapid evolution of cichlid fishes. *Science* **273**, 1091–1093 (1996).
43. L. K. Ayliffe, M. K. Gagan, J.-x. Zhao, R. N. Drysdale, J. C. Hellstrom, W. S. Hantoro, M. L. Griffiths, H. Scott-Gagan, E. S. Pierre, J. A. Cowley, B. W. Suwargadi, Rapid inter-hemispheric climate links via the Australasian monsoon during the last deglaciation. *Nat. Commun.* **4**, 2908 (2013).
44. S. van der Kaars, F. Bassinot, P. De Deckker, F. Guichard, Changes in monsoon and ocean circulation and the vegetation cover of southwest Sumatra through the last 83,000years: The record from marine core BAR94-42. *Palaeogeogr. Palaeoclimatol. Palaeoecol.* **296**, 52–78 (2010).
45. M. Mohtadi, S. Steinke, A. Lückge, J. Groeneveld, E. C. Hathorne, Glacial to Holocene surface hydrography of the tropical eastern Indian Ocean. *Earth Planet. Sci. Lett.* **292**, 89–97 (2010).
46. Y. Ruan, M. Mohtadi, S. van der Kaars, L. M. Dupont, D. Hebbeln, E. Schefuß, Differential hydro-climatic evolution of East Javanese ecosystems over the past 22,000 years. *Quat. Sci. Rev.* **218**, 49–60 (2019).
47. D. Yuan, H. Cheng, R. L. Edwards, C. A. Dykoski, M. J. Kelly, M. Zhang, J. Qing, Y. Lin, Y. Wang, J. Wu, Timing, duration, and transitions of the last interglacial Asian monsoon. *Science* **304**, 575–578 (2004).
48. Y. J. Wang, H. Cheng, R. L. Edwards, Z. S. An, J. Y. Wu, C. C. Shen, J. A. Dorale, A high-resolution absolute-dated late pleistocene monsoon record from Hulu Cave, China. *Science* **294**, 2345–2348 (2001).
49. F. S. Pausata, D. S. Battisti, K. H. Nisancioglu, C. M. Bitz, Chinese stalagmite $\delta^{18}O$ controlled by changes in the Indian monsoon during a simulated Heinrich event. *Nat. Geosci.* **4**, 474–480 (2011).
50. S. Lewis, A. LeGrande, M. Kelley, G. Schmidt, Water vapour source impacts on oxygen isotope variability in tropical precipitation during Heinrich events. *Clim. Past* **6**, 325–343 (2010).
51. E. Brady, S. Stevenson, D. Bailey, Z. Liu, D. Noone, J. Nusbaumer, B. L. Otto-Bliesner, C. Tabor, R. Tomas, T. Wong, J. Zhang, J. Zhu, The connected isotopic water cycle in the community earth system model version 1. *J. Adv. Model. Earth Syst.* **11**, 2547–2566 (2019).
52. W. R. Peltier, D. F. Argus, R. Drummond, Space geodesy constrains ice age terminal deglaciation: The global ICE-6G_C (VM5a) model. *J. Geophys. Res. Solid Earth* **120**, 450–487 (2015).
53. D. Lüthi, M. Le Floch, B. Bereiter, T. Blunier, J.-M. Barnola, U. Siegenthaler, D. Raynaud, J. Jouzel, H. Fischer, K. Kawamura, T. F. Stocker, High-resolution carbon dioxide concentration record 650,000–800,000 years before present. *Nature* **453**, 379–382 (2008).
54. J. R. Petit, J. Jouzel, D. Raynaud, N. I. Barkov, J. M. Barnola, I. Basile, M. Bender, J. Chappellaz, M. Davis, G. Delaygue, M. Delmotte, V. M. Kotlyakov, M. Legrand, V. Y. Lipenkov, C. Lorius, L. PÉpin, C. Ritz, E. Saltzman, M. Stievenard, Climate and atmospheric history of the past 420,000 years from the Vostok ice core, Antarctica. *Nature* **399**, 429–436 (1999).
55. A. Schilt, M. Baumgartner, T. Blunier, J. Schwander, R. Spahni, H. Fischer, T. F. Stocker, Glacial–Interglacial and millennial-scale variations in the atmospheric nitrous oxide concentration during the last 800,000 years. *Quat. Sci. Rev.* **29**, 182–192 (2010).
56. Z. Liu, B. L. Otto-Bliesner, F. He, E. C. Brady, R. Tomas, P. U. Clark, A. E. Carlson, J. Lynch-Stieglitz, W. Curry, E. Brook, D. Erickson, R. Jacob, J. Kutzbach, J. Cheng, Transient simulation of last deglaciation with a new mechanism for bolling-allerod warming. *Science* **325**, 310–314 (2009).
57. S. Stevenson, B. Otto-Bliesner, E. Brady, J. Nusbaumer, C. Tabor, R. Tomas, D. Noone, Z. Liu, Volcanic eruption signatures in the isotope-enabled last millennium ensemble. *Paleoceanogr. Paleoclimatol.* **34**, 1534–1552 (2019).
58. R. F. Adler, G. J. Huffman, A. Chang, R. Ferraro, P.-P. Xie, J. Janowiak, B. Rudolf, U. Schneider, S. Curtis, D. Bolvin, A. Gruber, J. Susskind, P. Arkin, E. Nelkin, The version-2 global precipitation climatology project (GPCP) monthly precipitation analysis (1979–present). *J. Hydrometeorol.* **4**, 1147–1167 (2003).

59. T. J. Heaton, P. Köhler, M. Butzin, E. Bard, R. W. Reimer, W. E. N. Austin, C. Bronk Ramsey, P. M. Grootes, K. A. Hughen, B. Kromer, P. J. Reimer, J. Adkins, A. Burke, M. S. Cook, J. Olsen, L. C. Skinner, Marine20—The marine radiocarbon age calibration curve (0–55,000 cal BP). *Radiocarbon* **62**, 779–820 (2020).
60. P. J. Reimer, W. E. N. Austin, E. Bard, A. Bayliss, P. G. Blackwell, C. B. Ramsey, M. Butzin, H. Cheng, R. L. Edwards, M. Friedrich, P. M. Grootes, T. P. Guilderson, I. Hajdas, T. J. Heaton, A. G. Hogg, K. A. Hughen, B. Kromer, S. W. Manning, R. Muscheler, J. G. Palmer, C. Pearson, J. van der Plicht, R. W. Reimer, D. A. Richards, E. M. Scott, J. R. Southon, C. S. M. Turney, L. Wacker, F. Adolphi, U. Büntgen, M. Capano, S. M. Fahrni, A. Fogtmann-Schulz, R. Friedrich, P. Köhler, S. Kudsk, F. Miyake, J. Olsen, F. Reinig, M. Sakamoto, A. Sookdeo, S. Talamo, The IntCal20 Northern Hemisphere Radiocarbon Age Calibration Curve (0–55 cal kBP). *Radiocarbon* **62**, 725–757 (2020).
61. M. Blaauw, J. A. Christen, Flexible paleoclimate age-depth models using an autoregressive gamma process. *Bayesian Anal.* **6**, 457–474 (2011).
62. A. Vincens, G. Buchet, D. Williamson, M. Taieb, A 23,000 yr pollen record from Lake Rukwa (8°S, SW Tanzania): New data on vegetation dynamics and climate in Central Eastern Africa. *Rev. Palaeobot. Palynol.* **137**, 147–162 (2005).
63. J. C. Stager, P. A. Mayewski, L. D. Meeker, Cooling cycles, Heinrich event 1, and the desiccation of Lake Victoria. *Palaeogeogr. Palaeoclimatol. Palaeoecol.* **183**, 169–178 (2002).
64. E. Parzen, On estimation of a probability density function and mode. *Ann. Math. Stat.* **33**, 1065–1076 (1962).
65. P. Barker, D. Williamson, F. Gasse, E. Gibert, Climatic and volcanic forcing revealed in a 50,000-year diatom record from Lake Massoko, Tanzania. *Quatern. Res.* **60**, 368–376 (2003).
66. K. Costa, J. Russell, B. Konecky, H. Lamb, Isotopic reconstruction of the African Humid Period and Congo Air Boundary migration at Lake Tana, Ethiopia. *Quat. Sci. Rev.* **83**, 58–67 (2014).
67. S. Garelick, J. M. Russell, S. Dee, D. Verschuren, D. O. Olago, Atmospheric controls on precipitation isotopes and hydroclimate in high-elevation regions in Eastern Africa since the Last Glacial Maximum. *Earth Planet. Sci. Lett.* **567**, 116984 (2021).
68. J. E. Tierney, J. M. Russell, J. S. Sinninghe Damsté, Y. Huang, D. Verschuren, Late quaternary behavior of the East African monsoon and the importance of the Congo Air Boundary. *Quat. Sci. Rev.* **30**, 798–807 (2011).
69. J. E. Tierney, P. B. DeMenocal, Abrupt shifts in Horn of Africa hydroclimate since the last glacial maximum. *Science* **342**, 843–846 (2013).
70. J. D. Shakun, S. J. Burns, D. Fleitmann, J. Kramers, A. Matter, A. Al-Subary, A high-resolution, absolute-dated deglacial speleothem record of Indian Ocean climate from Socotra Island, Yemen. *Earth Planet. Sci. Lett.* **259**, 442–456 (2007).
71. G. Windler, J. E. Tierney, J. Zhu, C. J. Poulsen, Unraveling glacial hydroclimate in the Indo-Pacific Warm Pool: Perspectives from water isotopes. *Paleoceanogr. Paleoclimatol.* **35**, e2020PA003985 (2020).
72. S. A. Wicaksono, J. M. Russell, A. Holbourn, W. Kuhnt, Hydrological and vegetation shifts in the Wallacean region of central Indonesia since the Last Glacial Maximum. *Quat. Sci. Rev.* **157**, 152–163 (2017).
73. B. Konecky, J. Russell, S. Bijaksana, Glacial aridity in central Indonesia coeval with intensified monsoon circulation. *Earth Planet. Sci. Lett.* **437**, 15–24 (2016).
74. S. Weldeab, D. W. Lea, H. Oberhänsli, R. R. Schneider, Links between southwestern tropical Indian Ocean SST and precipitation over southeastern Africa over the last 17kyr. *Palaeogeogr. Palaeoclimatol. Palaeoecol.* **410**, 200–212 (2014).
75. Y. V. Wang, G. Leduc, M. Regenberg, N. Andersen, T. Larsen, T. Blanz, R. R. Schneider, Northern and southern hemisphere controls on seasonal sea surface temperatures in the Indian Ocean during the last deglaciation. *Paleoceanography* **28**, 619–632 (2013).
76. N. Rippert, K.-H. Baumann, J. PÄTzold, Thermocline fluctuations in the western tropical Indian Ocean during the past 35 ka. *J. Quat. Sci.* **30**, 201–210 (2015).
77. S. Romahn, A. Mackensen, J. Groeneveld, J. Pätzold, Deglacial intermediate water reorganization: New evidence from the Indian Ocean. *Climate Past* **10**, 293–303 (2014).
78. H. J. H. Johnstone, T. Kiefer, H. Elderfield, M. Schulz, Calcite saturation, foraminiferal test mass, and Mg/Ca-based temperatures dissolution corrected using XDX—A 150 ka record from the western Indian Ocean. *Geochemistry Geophys. Geosystems* **15**, 781–797 (2014).
79. F. Rostek, E. Bard, L. Beaufort, C. Sonzogni, G. Ganssen, Sea surface temperature and productivity records for the past 240 kyr in the Arabian Sea. *Deep Sea Res. Part II Top. Stud. Oceanogr.* **44**, 1461–1480 (1997).
80. E. Bard, F. Rostek, C. Sonzogni, Interhemispheric synchrony of the last deglaciation inferred from alkenone palaeothermometry. *Nature* **385**, 707–710 (1997).
81. C. Huguet, J. H. Kim, J. S. Sinninghe Damsté, S. Schouten, Reconstruction of sea surface temperature variations in the Arabian Sea over the last 23 kyr using organic proxies (TEX_{86} and $U37^{K'}$). *Paleoceanography* **21**, PA3003 (2006).
82. D. Budziak, Late Quaternary monsoonal climate and related variations in paleoproductivity and alkenone-derived sea-surface temperatures in the western Arabian Sea. *Berichte, Fachbereich Geowissenschaften, Universität Bremen* (2001).
83. P. Govil, P. D. Naidu, Evaporation-precipitation changes in the eastern Arabian Sea for the last 68 ka: Implications on monsoon variability. *Paleoceanography* **25**, PA1210 (2010).
84. R. Saraswat, D. W. Lea, R. Nigam, A. Mackensen, D. K. Naik, Deglaciation in the tropical Indian Ocean driven by interplay between the regional monsoon and global teleconnections. *Earth Planet. Sci. Lett.* **375**, 166–175 (2013).
85. S. Liu, W. Ye, M.-T. Chen, H.-J. Pan, P. Cao, H. Zhang, S. Khokiattiwong, N. Kornkanitnan, X. Shi, Millennial-scale variability of Indian summer monsoon during the last 42 kyr: Evidence based on foraminiferal Mg/Ca and oxygen isotope records from the central Bay of Bengal. *Palaeogeogr. Palaeoclimatol. Palaeoecol.* **562**,110112(2021), 110112.
86. H. R. Kudrass, A. Hofmann, H. Doose, K. Emeis, H. Erlenkeuser, Modulation and amplification of climatic changes in the Northern Hemisphere by the Indian summer monsoon during the past 80 k.y. *Geology* **29**, 63–66 (2001).
87. S. Liu, W. Ye, P. Cao, H. Zhang, M.-T. Chen, X. Li, J. Li, H.-J. Pan, S. Khokiattiwong, N. Kornkanitnan, X. Shi, Paleoclimatic responses in the tropical Indian Ocean to regional monsoon and global climate change over the last 42 kyr. *Mar. Geol.* **438**, 106542 (2021).
88. X. Wang, Z. Jian, A. Lückge, Y. Wang, H. Dang, M. Mohtadi, Precession-paced thermocline water temperature changes in response to upwelling conditions off southern Sumatra over the past 300,000 years. *Quat. Sci. Rev.* **192**, 123–134 (2018).
89. R. Y. Setiawan, M. Mohtadi, J. Southon, J. Groeneveld, S. Steinke, D. Hebbeln, The consequences of opening the Sunda Strait on the hydrography of the eastern tropical Indian Ocean. *Paleoceanography* **30**, 1358–1372 (2015).
90. S. Steinke, H.-Y. Chiu, P.-S. Yu, C.-C. Shen, H. Erlenkeuser, L. Löwemark, M.-T. Chen, On the influence of sea level and monsoon climate on the southern South China Sea freshwater budget over the last 22,000 years. *Quat. Sci. Rev.* **25**, 1475–1488 (2006).
91. W. Fan, Z. Jian, Z. Chu, H. Dang, Y. Wang, F. Bassinot, X. Han, Y. Bian, Variability of the Indonesian Throughflow in the Makassar Strait over the last 30 ka. *Sci. Rep.* **8**, 5678 (2018).
92. J. F. Schröder, W. Kuhnt, A. Holbourn, S. Beil, P. Zhang, M. Hendrizan, J. Xu, Deglacial warming and hydroclimate variability in the central Indonesian archipelago. *Paleoceanogr. Paleoclimatol.* **33**, 974–993 (2018).
93. C. Levi, L. Labeyrie, F. Bassinot, F. Guichard, E. Cortijo, C. Waelbroeck, N. Caillon, J. Duprat, T. de Garidel-Thoron, H. Elderfield, Low-latitude hydrological cycle and rapid climate changes during the last deglaciation. *Geochem. Geophys. Geosytems* **8**, Q05N12 (2007).
94. F. T. Gibbons, D. W. Oppo, M. Mohtadi, Y. Rosenthal, J. Cheng, Z. Liu, B. K. Linsley, Deglacial δ18O and hydrologic variability in the tropical Pacific and Indian Oceans. *Earth Planet. Sci. Lett.* **387**, 240–251 (2014).
95. Y. Rosenthal, D. W. Oppo, B. K. Linsley, The amplitude and phasing of climate change during the last deglaciation in the Sulu Sea, western equatorial Pacific. *Geophys. Res. Lett.* **30**, 1428 (2003).
96. J. Xu, A. Holbourn, W. Kuhnt, Z. Jian, H. Kawamura, Changes in the thermocline structure of the Indonesian outflow during Terminations I and II. *Earth Planet. Sci. Lett.* **273**, 152–162 (2008).
97. T. Bolliet, A. Holbourn, W. Kuhnt, C. Laj, C. Kissel, L. Beaufort, M. Kienast, N. Andersen, D. Garbe-Schönberg, Mindanao Dome variability over the last 160 kyr: Episodic glacial cooling of the West Pacific warm pool. *Paleoceanography* **26**, PA1208 (2011).
98. A. Holbourn, W. Kuhnt, J. Xu, Indonesian Throughflow variability during the last 140 ka: The Timor Sea outflow. *Geol. Soc. Spec. Publ.* **355**, 283–303 (2011).
99. Z. Jian, Y. Wang, H. Dang, D. W. Lea, Z. Liu, H. Jin, Y. Yin, Half-precessional cycle of thermocline temperature in the western equatorial Pacific and its bihemispheric dynamics. *Proc. Natl. Acad. Sci. U.S.A.* **117**, 7044–7051 (2020).
100. M. Mohtadi, A. Lückge, S. Steinke, J. Groeneveld, D. Hebbeln, N. Westphal, Late Pleistocene surface and thermocline conditions of the eastern tropical Indian Ocean. *Quat. Sci. Rev.* **29**, 887–896 (2010).
101. M. Mohtadi, M. Prange, E. Schefuss, T. C. Jennerjahn, Late Holocene slowdown of the Indian Ocean Walker circulation. *Nat. Commun.* **8**, 1015 (2017).
102. A. Rajasree, V. R. Punyu, V. K. Banakar, Last 35,000-year water column temperature and productivity variation in the Eastern Arabian Sea: Monsoon and global climate connection. *Geo-Marine Lett.* **39**, 239–248 (2019).

Acknowledgments: We would like to thank the editor, Dr. Kaustubh Thirumalai and an anonymous reviewer for their comments and suggestions, which helped improve this manuscript. **Funding:** This work was supported by the Voss Postdoctoral Fellowship at Brown University, Institute at Brown for Environment and Society (X.D.), NSF-P2C2 2202746 (X.D.), NSF-EAR 2102856 (J.M.R.), and NSF-AGS 1656907 (Z.L.); Deutsche Forschungsgemeinschaft (DFG) grant MO2546/3–1 (M.M.); and Joint Initiative Awards fund from the Andrew W. Mellon Foundation (D.W.O.). **Author contributions:** Conceptualization: J.M.R. and X.D. Formal analysis: X.D. Funding acquisition: X.D., J.M.R., Z.L., and M.M. Investigation: X.D., J.M.R., Z.L., B.L.O.-B.,

D.W.O., M.M., C.Z., Y.G., V.V.G., N.D., and J.A. Methodology: X.D., J.M.R., Z.L., and B.L.O.-B. Resources: J.M.R., Z.L., B.L.O.-B., D.W.O., M.M., and Y.R. Visualization: X.D. Supervision: J.M.R. Project administration: J.M.R. and X.D. Writing—original draft: X.D. Writing—review and editing: X.D., J.M.R., Z.L., B.L.O.-B., D.W.O., M.M., C.Z., V.V.G., E.S., Y.Y., Y.R., N.D., J.A., and Y.G. **Competing interests:** The authors declare that they have no competing interests. **Data and materials availability:** The proxy data synthesized in this work are available from the PANGAEA database (https://pangaea.de/) and NOAA's National Climatic Data Center's Paleoclimatology database (http://ncdc.noaa.gov/paleo/paleo.html). The model simulation results are available at NCAR Climate Data Gateway (https://www.earthsystemgrid.org. All data needed to evaluate the conclusions in the paper are present in the paper and/or the Supplementary Materials.

Submitted 23 June 2022
Accepted 23 November 2022
Published 4 January 2023
10.1126/sciadv.add4909